

System Identification Flight Testing of Inverted V-Tail Small Unmanned Air System

Christopher Leshikar*, Scott Gosnell[†], Esteban Gomez[‡], Luke Moy[§] and John Valasek[¶] *Texas A&M University, College Station, TX, 77843-3141*

This paper presents an approach for generating linear time invariant state-space models of a small Unmanned Air System. An instrumentation system using the robot operating system with commercial-off-the-shelf components is implemented to record flight data and inject automated excitation signals. Offline system identification is conducted using the Observer/Kalman Identification algorithm to produce a discrete-time linear time invariant state-space model, which is then converted to a continuous time-model for analysis. Challenges concerning data collection and inverted V-Tail modelling are discussed, and solutions are presented. Longitudinal, lateral/directional and combined longitudinal lateral/directional models of the test vehicle are generated using both manual and automated excitations, and are presented and compared. The generated longitudinal and lateral/directional results are compared to results for a small Unmanned Air System with a standard empennage. Flight test results presented in the paper show decent matching between the decoupled longitudinal and lateral/directional model and the combined longitudinal/lateral directional model.

I. Nomenclature

 \mathbf{x} = State vector

y = Measurement vector

 \bar{A} = Augmented observer system matrix

 \bar{B} = Augmented observer input matrix

v = Stacked input and output vector

G = Arbitrary matrix

 \bar{y} = Augmented measurement vector

 \bar{Y} = Observer Markov Parameters (OMP)

 \bar{V} = Stacked input and output matrix

p = Number of time shifts in the Hankel matrices

H = Hankel matrix

 \hat{A} = Identified system matrix

 \hat{B} = Identified input matrix

 \hat{C} = Identified output matrix

 \hat{D} = Identified carry-through matrix

u(t) = Signal

 A_k = Amplitude

 ϕ_k = Phase shift

 ω_n = Natural Frequency, rad/sec

 τ = Time Constant, sec

^{*}Graduate Research Assistant, Vehicle Systems & Control Laboratory, Aerospace Engineering Department. Student Member AIAA. cilesh@tamu.edu.

[†]Graduate Research Assistant, Vehicle Systems & Control Laboratory, Aerospace Engineering Department. Student Member AIAA. scott.gos@tamu.edu.

[‡]Graduate Research Assistant, Vehicle Systems & Control Laboratory, Aerospace Engineering Department. Student Member AIAA. esteban.gomez98tamu.edu.

[§]Undergraduate Research Assistant, Vehicle Systems & Control Laboratory, Aerospace Engineering Department. Student Member AIAA. lukemov1999@tamu.edu.

[¶]Professor and Director, Vehicle Systems & Control Laboratory, Aerospace Engineering Department. Fellow AIAA. valasek@tamu.edu, http://vscl.tamu.edu/valasek

 ζ = Damping Ratio α = Angle-of-attack, deg β = Sideslip angle, deg ϕ, θ = Euler attitude angles, deg δ_a = Aileron deflection, deg

 δ_e = Elevator deflection, deg δ_r = Rudder deflection, deg

 δ_t = Throttle command, fraction of maximum throttle

II. Introduction

Flight vehicles can be modeled as linear state-space systems describing perturbed motion around a trim point (i.e. an equilibrium condition of the full nonlinear system) as shown in Eq. [1]:

$$\dot{\mathbf{x}} = A(t)\mathbf{x}(t) + B\mathbf{u}(t)$$

$$\mathbf{y}(t) = C(t)\mathbf{x}(t) + D(t)\mathbf{u}(t)$$
(1)

where $x \in \mathbb{R}^n$ is the perturbed state vector, $u \in \mathbb{R}^m$ is a perturbed control vector, and $y \in \mathbb{R}^p$ is the perturbed output vector. The state matrix $A \in \mathbb{R}^{n \times n}$, control influence matrix $B \in \mathbb{R}^{n \times m}$, output matrix $C \in \mathbb{R}^{p \times n}$, and carry-through matrix $D \in \mathbb{R}^{p \times m}$ describe the system. If the 4-tuple (A, B, C, D) is independent of time it is a Linear Time Invariant (LTI) system. Several methods exist to generate flight models which vary in complexity and fidelity. Empirical techniques and linear aerodynamics \mathbb{I} can be used to generate low-fidelity models which are useful for preliminary design work \mathbb{I} . These methods produce errors in the 10-20% range for the most critical parameters. Aerodynamic prediction codes are then typically used to populate aerodynamic databases across the flight envelope \mathbb{I} . Models that are generated by wind tunnel testing are used to verify and validate the lower fidelity computational models. Lastly, experimental flight testing can be performed to generate the highest fidelity model. This method is the most expensive however.

There are a variety of algorithms available for generating models from data obtained from flight testing. Such algorithms include the Eigensystem Realization Algorithm (ERA) [5], Observer/Kalman Identification (OKID) [6], the Comprehensive Identification from Frequency Responses (CIFER®) algorithm [7], Free Response Functions [8], and Observer/Controller Identification (OCID) [9]. A historical overview of flight vehicle system identification approaches is presented by Hamel [10]. Previous work of the authors include using OKID for system identification of flight vehicles [11]-15]. A commercial-off-the-shelf (COTS), low size, weight, power, and cost (SWaP-C) Developmental Flight Test Instrumentation (DFTI) system is developed and implemented by the authors in [16]. The 100 Hz sampling makes it an ideal instrumentation system for system identification and modeling applications. A flight test instrumentation system based in the Robot Operating System (ROS) is developed and implemented in by the authors in [15]. The ROS based system, the Developmental Flight Test Instrumentation System Two (DFTI2), collects data at 100 Hz and allows users to inject specified signals to the control surfaces similar to the DFTI system presented in [16]. This work implements the DFTI2 system in [15] on an inverted V-Tail sUAS and presents a testing approach for system identification flight testing.

The paper is organized as follows. Section III introduces the airframe and hardware implemented on the airframe. Section IV details the theoretical development of OKID which is used for generating discrete linear state-space models. The Developmental Flight Test Instrumentation Two is presented in Section III Implementation Challenges for system identification flight testing on the vehicle are presented in Section III discusses the approach for selecting the excitation signals. The results from flight tests and the quality indicators used are presented in Section IX presents the conclusions and recommendations for future work.

III. Test Vehicle

The RMRC Anaconda is a fixed-wing small Unmanned Air System (sUAS) produced by Ready Made RC. The Anaconda is excellent for low speed flights, and is rugged enough to endure short takeoffs and landings during testing. Previous system identification work on this type of vehicle includes the identification of a longitudinal model [17]. The foam build of the aircraft can easily support different configurations and placements of sensors within the fuselage, and makes it light and durable, ideal for extended flights. Figure 1 shows the Anaconda that is used for the flight tests.

Table 1 Hardware Specifications

Avionics

Avionics					
Autopilot	Pixhawk 2.1 Blue Cube				
Triple Redundant IMU	InvenSense MPU9250 (First)				
	MPU9250 (Third)				
	LSM303D (Backup)				
MPU9250 IMU					
Gyro Full Scale Range	±250 / ±500 / ±1000 / ±2000 °/sec				
Gyro Rate Noise	0.01 mdps/rtHz				
Accelerometer Full Scale Range	±2 g / ±4 g / ±6 g / ±8 g / ±16 g				
Accelerometer Sensitivity	±4800LSB/g				
LSM303D IMU					
Accelerometer Full Scale Range	±2 g / ±4 g / ±6 g / ±8 g / ±16 g				
Magnetometer Full Scale Range	$\pm 2 / \pm 4 / \pm 8 / \pm 12$ gauss				
IMU Operating Temperatures	-10°C to 55°C				
Instrumentation Computer	Jetson Nano Developer Kit				
RAM	4GB DDR SDRAM				
Processor	Quad-core ARM A57 CPU				
GPS System	Here2 GPS				
Sensitivities					
Tracking & Navigation	-167dBm				
Hot Start	-148dBm				
Cold Start	-157dBm				
Micro-Controller	Arduino Mega 2560				
Flash memory	256 KB				
SRAM	8 KB				
Clock Speed	16 MHz				
Pitot Tube & Differential Pressure Sensor	Pixhawk Digital Airspeed Sensor				
Operating Pressure	1 psi (Airspeed up to 100 m/s)				
Accuracy	±0.25%				
Resolution	$1.218 \times 10^{-4} \text{ psi}$				

The test vehicle possesses a wingspan of 6.75 feet with dual booms and an inverted V-tail pusher design. The aircraft has an empty weight of 5.55 pounds, and has an endurance of 15-20 minutes. The propulsion system used for the aircraft includes a T-Motor AT3520-5 KV880 Brushless motor, a Castle 80A HV Electronic Speed Controller, and an APC 13x8E propeller. The ailerons are powered by SpringRC SM-S3483 Metal Gear servos, and the ruddervators are powered by HiTech HS-5085MG digital micro servos.



Fig. 1 RMRC Anaconda with test instrumentation

IV. Observer / Kalman Filter Identification

The Observer/Kalman Filter Identification (OKID) method is a direct Kalman filter gain approach that is formulated in the time-domain and is capable of handling general response data [8]. Because pure impulse excitations are difficult to apply to air vehicles and the noise/signal ratio of sensing data are usually high it is especially valuable for air vehicle modeling. It also allows for nonzero initial conditions and does not require the response to reach steady-state before data collection. OKID was originally developed for elastic spacecraft but has been successfully used to identify state-space models of air vehicles [18], [16]. Because OKID only requires input/output time histories to perform system identification the amount of a priori system specific information is reduced.

The development of the OKID algorithm here generally follows [18]. Starting with linearized, discrete-time, state-space equations augmented with an observer gain:

$$x(k+1) = \bar{A}x(k) + \bar{B}v(k)$$

$$y(k) = Cx(k) + Du(k)$$
(2)

where $x(k) \in \mathbb{R}^n$, $y(k) \in \mathbb{R}^m$, $u(k) \in \mathbb{R}^r$, are state, output, and control inputs with

$$\bar{A} = A + GC$$

$$\bar{B} = [B + GD, -G]$$

$$v(k) = \begin{bmatrix} u(k) \\ y(k) \end{bmatrix}$$
(3)

and $G \in \mathbb{R}^{n \times m}$ is an arbitrary matrix chosen to make the matrix \bar{A} stable. Assuming zero initial conditions and integer p satisfying $CA^kB \approx 0$ for $k \ge p$, substituting and iterating through each time step using Equation (2), the Observer Markov Parameters (OMP) comprised of a input-output relationship becomes

$$\bar{\mathbf{y}} = C\bar{A}^p \mathbf{x} + \bar{Y}\bar{V} \tag{4}$$

where

$$\bar{y} = \begin{bmatrix} y(p) & y(p+1) & \cdots & y(l-1) \end{bmatrix} \\
\bar{Y} = \begin{bmatrix} D & C\bar{B} & C\bar{A}\bar{B} & \cdots & C\bar{A}^{(p-1)}\bar{B} \end{bmatrix} \\
\bar{V} = \begin{bmatrix} u(p) & u(p+1) & \cdots & u(l-1) \\ v(p-1) & v(p) & \cdots & v(l-2) \\ v(p-2) & v(p-1) & \cdots & v(l-3) \\ \vdots & \ddots & \ddots & \vdots \\ v(0) & v(1) & \cdots & v(l-p-1) \end{bmatrix}$$
(5)

The matrix \bar{Y} is partitioned with the system Markov parameters such that

$$\bar{Y} = \left[D \ C\bar{B} \ C\bar{A}\bar{B} \ \cdots \ C\bar{A}^{(p-1)}\bar{B} \right] = \left[Y_0 \ Y_1 \ Y_2 \ \cdots Y_p \right] \tag{6}$$

from which the OMP are obtained.

$$\bar{Y}_{0} = D$$

$$\bar{Y}_{k} = C\bar{A}^{(k-1)}\bar{B}$$

$$= \left[C(A+GC)^{(k-1)}(B+GD) - C(A+GC)^{(k-1)}G\right]$$

$$= \left[\bar{Y}_{k}^{(1)} - \bar{Y}_{k}^{(2)}\right] \quad k = 1, 2, 3, ...$$
(7)

The general relationship between the actual system Markov parameters and the OMP can be shown to be

$$D = Y_0 = \bar{Y}_0$$

$$Y_k = Y_k^{(1)} - \sum_{i=1}^k \bar{Y}_i^{(2)} Y_{(k-i)} \quad \text{for } k = 1, \dots, p$$

$$Y_k = -\sum_{i=1}^p \bar{Y}_i^{(2)} Y_{(k-i)} \quad \text{for } k = p + 1, \dots, \infty$$
(8)

The next step is to use a singular value decomposition (SVD) on the Hankel matrix:

$$H(k-1) = \begin{bmatrix} Y_{k} & Y_{k+1} & \cdots & Y_{k+\beta-1} \\ Y_{k+1} & Y_{k+2} & \cdots & Y_{k+\beta} \\ \vdots & \vdots & \ddots & \vdots \\ Y_{k+\alpha-1} & Y_{k+\alpha} & \cdots & Y_{k+\alpha+\beta-2} \end{bmatrix}$$

$$H(0) = P_{n} \sum O_{n}$$
(9)

The ERA is then used to solve the Hankel matrix for the desired state-space realization (A, B, C, D):

$$\hat{A} = \sum_{n}^{-1/2} P_{n} H(1) Q_{n} \sum_{n}^{-1/2} \hat{B} = \sum_{n}^{1/2} Q_{n}$$

$$\hat{C} = P_{n} \sum_{n}^{1/2} \hat{D} = Y_{0}$$
(10)

Note that \hat{A} , \hat{B} , and \hat{C} are the estimated system matrices determined using OKID. The 4-tuple $(\hat{A}, \hat{B}, \hat{C}, \hat{D})$ represent the identified discrete linear state-space system:

$$\mathbf{x}(k+1) = \hat{A}\mathbf{x}(k) + \hat{B}\mathbf{u}(k)$$

$$\mathbf{y}(k) = \hat{C}\mathbf{x}(k) + \hat{D}\mathbf{u}(k)$$
(11)

V. Developmental Flight Test Instrumentation Two

The capabilities of COTS autopilots have improved greatly, meaning modern flight controllers are now able to log relevant parameters at over 100 Hz. This enhanced capability greatly simplifies the data logging process. The Developmental Flight Test Instrumentation Two (DFTI2) is the instrumentation system used for this work. DFTI2 is based in the robot operating system (ROS), and contains two ROS nodes: one for data logging and one for injecting automated excitations. The data is collected at a sampling rate of 100 Hz. For the RMRC Anaconda, the following hardware is used for the DFTI2 system: a Pixhawk 2.1 Blue Cube by Cube Pilot, an Arduino Mega 2560 microcontroller and a Jetson Nano. The Jetson Nano is used as a companion computer which runs DFTI2. The Pixhawk Blue Cube is

used to collected state measurement data as well as the throttle input. The Arduino Mega 2560 measures the control surface deflections. A detailed discussion of the hardware and software architecture of the DFTI2 system is presented in 15. One major update of the DFTI2 system since 15 is the implementing of automated Schroeder sine sweeps. The following Schroeder sine sweep 19 is implemented in DFTI2

$$u(t) = \sum_{k=1}^{M} A_k \cos(\frac{2\pi k \tau(t)}{T} + \phi_k, t = 0, 1, ..., N - 1)$$

$$A_k = \sqrt{\frac{P}{M}}$$

$$\phi_1 = 0$$

$$\phi_k = \phi_{k-1} - \frac{\pi k^2}{N}, k = 2, 3, ..., M$$
(12)

where M is the number of harmonically related excitation frequencies. A procedure is shown in [20] to select the excitation frequencies such that the Schroeder sine sweep can be effectively implemented for concurrent control surface excitations.

VI. Implementation Challenges

Several challenges arise in preparing the RMRC Anaconda for system identification test flights. The challenges arise in two areas: collection the necessary data to perform system identification and modelling of the inverted V-tail.

A. Data Collection

The RMRC Anaconda has a max takeoff weight of 13 lbs. The vehicle has an empty weight of 5.5 lbs, leaving 7.5 lbs for instrumentation. Furthermore there is limited space in the interior of the vehicle. This limits the sensors that may be placed on the vehicle. The test vehicle used in $\boxed{14}$ possesses the necessary interior space to carry a 5-hole probe which measures angle-of-attack α and sideslip angle β directly. Such a sensor will not fit on the test vehicle used in this work. Therefore α and β are estimated using small angle approximations. Another challenge in data collection is measuring the control surface deflections. It is possible to measure the pulse width modulation (PWM) values going to each servo but this approach has several drawbacks. One issue is that range PWM values to not transfer well from vehicle to vehicle. The range of PWM values vary between vehicles due to hardware imperfections, transmitter settings and RC calibrations for Flight Control Units such as the Pixhawk 2.1 Blue Cube. Additionally, measuring the PWM values going into the servos neglects the actuator dynamics of the servos. This can be an issue if it becomes necessary to change out the servos on the vehicle, which occurs in this work.

For larger UAS, voltage pots may be installed to measure control surface deflections [14]. For sUAS such as the RMRC Anaconda this is not possible. Therefore control surface deflections are measured by using signal feedback wires from the servos. Standard servos for the sUAS are not setup for signal feedback. The signal feedback wires are setup as follows. First, the servo cover is taken off to expose the small circuit board inside the servo. Next, a wire is soldered onto the circuit board such that it is connected to the signal wire coming from the FCU. Then the servo cover is secured back onto the servo. Lastly the signal feedback wire is connect to an analog port on an Arduino micro-controller. Figure 2 shows an modified feedback servo on the ruddervator of the test vehicle.



Fig. 2 Modified HS-225MG Servo for the Right Ruddervator

An issue arises when setting up the signal feedback wires for the ruddervators. The ruddervator servos have a small volume which makes it very difficult to make a good solder connection for the signal feedback wires. This challenge negatively affects the identified models generated from the flight data from flights before July 2021. To overcome this challenge, the ruddervator servos are changed from the HiTech HS-5085MG digital micro servos to the HiTech HS-225MG high performance mini servos. The HS-225MG servos have the same volume as the aileron servos while possessing only 4 oz-in more torque than the HS-5085MG. The change in ruddervator servos results in better signal feedback from the ruddervators without significantly changing the control power of the ruddervator servos. There is a drawback with this approach however. Power from the FCU is required when connecting the feedback wire to the port on micro-controller. This introduces significant noise into the control surface deflection data. Therefore more thought is required when implementing noise filtering.

B. Modelling of the Inverted V-Tail

The presence of coupled control surfaces presents a challenge when attempting to identify models. One of the issues is sign convention. The feedback wires measure the deflections of the ruddervators. For identifying models the ruddervator deflections are unmixed into the equivalent elevator and rudder deflections. The signs of the elements in the identified control influence matrix using unmixed signals can differ from those in an identified control influence using standard empennage control signals. This difference can come about from how the positive deflection for the inverted V-Tail is implemented. In this work, positive deflection for both ruddervators is defined as moving the ruddervators downward such that a pitch down motion is induced. Figure 3 shows positive elevator deflection. Therefore for a yaw right ruddervator deflection, the left ruddervator will deflect in the positive direction while the right ruddervator will deflect in the negative deflection. Figure 4 shows the yaw right deflection on the vehicle. Additionally, the presence of the ruddervators complicates the implementation of automated excitations. UAS with standard empennage configurations can inject elevator and rudder inputs simultaneously. This is very difficult to implement on an inverted V-Tail due to signal mixing. Elevator and rudder inputs are therefore injected sequentially rather than simultaneously when performing combined longitudinal lateral/directional excitations.



Fig. 3 Positive Elevator Deflection for the RMRC Anaconda



Fig. 4 Yaw Right Deflection for the RMRC Anaconda

VII. Testing Methodology

The selection of excitation signals is crucial to identifying a quality linear model. Selecting the proper set of inputs is difficult however. It is important to consider a wide range of excitation signals in terms of signal type, signal amplitude and signal period given that each aircraft requires a unique set of inputs. Therefore, considering a wide range of signals allows for the determination of the set of input models that best excite all the dynamic modes of the system. In this work, the following signal types are utilized: doublet, 3-2-1-1, sine sweep and Schroeder sine sweeps. Doublets and 3-2-1-1s are used due to being easy to implement. These signals have a lower success rate however. The sine sweep signal excites the largest range of frequencies but has the drawbacks of possibly exciting structural modes and causing control coupling in the identified model. Schroeder sine sweeps avoid the drawbacks of the sine sweeps but require basic *a priori* knowledge about the vehicle dynamics.

For this work, parameter sweeps of the excitation signals are considered. A parameter sweep for signal amplitude is defined for 2, 4, 6 and 8 degrees. It is found that signal amplitudes above 6 degrees knock the vehicle response into the nonlinear range, making it difficult to generate a quality linear state-space model. It is also found that signal amplitudes of 2 degrees struggle to properly excite the dynamic modes. Therefore a majority of automated excitations have an amplitude of 4 degrees. A parameter sweep for excitation signal length is also considered. The range of signal length sweep is 1, 2, 4 6 and 8 seconds. Table 2 shows the excitation maneuvers performed and considered in this paper. Early excitation maneuvers are injected manually by the pilot as the excitation node was not ready for flight operations at the time. The more recent excitation maneuvers are all automated by the excitation node discussed in Section 1 The excitation node provides the ability to perform a wider range of excitation signals rather than solely doublets. A total of 302 excitation maneuvers are performed and considered for this work.

Table 2 Excitation Maneuvers Performed

Date	Lateral/Directional	Longitudinal	Combined	Input Type	Manual	Automated
03/05/21	0	0	18	Doublet	X	
03/09/21	15	10	0	Doublet	Doublet X	
03/20/21	0	0	9	Doublet	X	
04/06/21	0	0	7	Doublet	X	X
04/19/21	0	0	19	Doublet	X	
06/02/21	7	0	0	Doublet		X
07/19/21	0	0	16	Doublet		X
07/21/21	0	0	5	Sine Sweep		X
07/28/21	7	7	0	3-2-1-1		X
08/05/21	10	10	10	Sine Sweep		X
08/23/21	10	0	0	Sine Sweep		X
08/24/21	0	10	10	Sine Sweep		X
08/30/21	10	10	10	Sine Sweep		X
09/09/21	11	10	11	Sine Sweep		X
11/02/21	10	10	10	Schroeder Sweep		X
11/19/21	10	10	10	Schroeder Sweep		X
Totals	90	77	135			

VIII. Flight Test Results

Flight tests are performed over sixteen flight days to collect data as seen in Table 2. A combination of lateral/directional (Lat/D), longitudinal (Lon), and combined Lon Lat/D maneuvers are performed. Both manual and automated excitation signals are used. All manual excitation maneuvers are chosen to be doublets of varying magnitudes and duration for δ_e , δ_a , δ_r and max-idle signals of varying duration for δ_t . Upwards of fifty-plus excitation maneuvers are performed using manual excitations. Two hundred and twenty-one automated excitation maneuvers are performed.

The ruddervator signals are unmixed by manipulating the mixing equations used by the Blue Cube to get pure elevator and rudder signals to make it as if the Anaconda has a standard empennage configuration. For the generation of models using OKID, a second-order Butterworth filter is applied state measurement data. The filtering for control surface deflections is more involved. The Arduino introduces some large spikes in the data. To remove this a filter is applied that removes data points where there is a large difference between the actual value and the expected value. A 15-point Spencer filter [21] is then applied to the control surface deflection data.

It is important to have some metric by which to judge the quality of an identified model. In this work the Mode Singular Value (MSV), Modal Controllability Index (MCI), and Modal Observability Index (MOI) are used as developed in [22]. These indicators are calculated by

$$MCI = 100 \cdot |B_m| \max |B_m|$$

$$MOI = 100 \cdot |C_m| \max |C_m|$$

$$MSV = 100 \cdot \frac{\frac{\sqrt{|B_m| \cdot |C_m|}}{|1 - |\zeta||}}{\max \frac{\sqrt{|B_m| \cdot |C_m|}}{|1 - |\zeta||}}$$
(13)

where $B_m \in \mathbb{R}^{nm \times r}$ is the modal input matrix, nm is the number of modes, $C_m \in \mathbb{R}^{m \times nm}$ is the modal output matrix, and $\zeta \in \mathbb{R}^{nm}$ is the eigenvalue vector. Theil Inequality Coefficients (TICs) are also used to determine quality of the model. The Theil Inequality Coefficient [21] is defined as

$$\mathcal{T}_{i} = \frac{\sqrt{\frac{1}{N} \sum_{k=1}^{N} \left[\hat{y}_{i}(k) - y_{i}(k)\right]^{2}}}{\sqrt{\frac{1}{N} \sum_{k=1}^{N} \left[\hat{y}_{i}(k)\right]^{2}} + \sqrt{\frac{1}{N} \sum_{k=1}^{N} \left[y_{i}(k)\right]^{2}}} \quad i = 1, 2, \dots, N$$
(14)

where y_i is the ith state measurement and \hat{y}_i is the ith state measurement estimated by the identified model. An averaged TIC value for an identified model can be obtained by taking the average of the TICs for each state measurement. TICs can have a value between 0 and 1 with 0 indicating perfect matching. A model with an averaged TIC value of less than 0.3 may be considered a good model.

A. Longitudinal

Table 3 shows the identified longitudinal model. An automated Schroeder sine sweep is injected into the elevator for 4 seconds after a max-idle signal is injected into the throttle. The standard dynamic modes are identified. This result differs from 17 in which the non-standard modes longitudinal modes are identified. OKID identifies both the short period and phugoid well, with MSVs of 100.0% and 58.9% respectively. Figure 5 shows the control inputs and state responses used to identify the model in Table 3. It is seen that the identified model tracks the flight data well. The averaged TIC value is calculate to be 0.153, indicating that the identified model is a good linear model.

Table 3 Identified Longitudinal Anaconda Model

Mode	Eigenvalue	ω_n (rad/sec)	ζ	τ (sec)	MSV (%)	MCI (%)	MOI (%)
Short Period	$-0.0853 \pm j1.2363$	1.2393	0.1830	_	100.0	100.0	92.3
Phugoid	$-0.0752 \pm j0.4039$	0.4109	0.0688	_	58.9	36.4	100.0

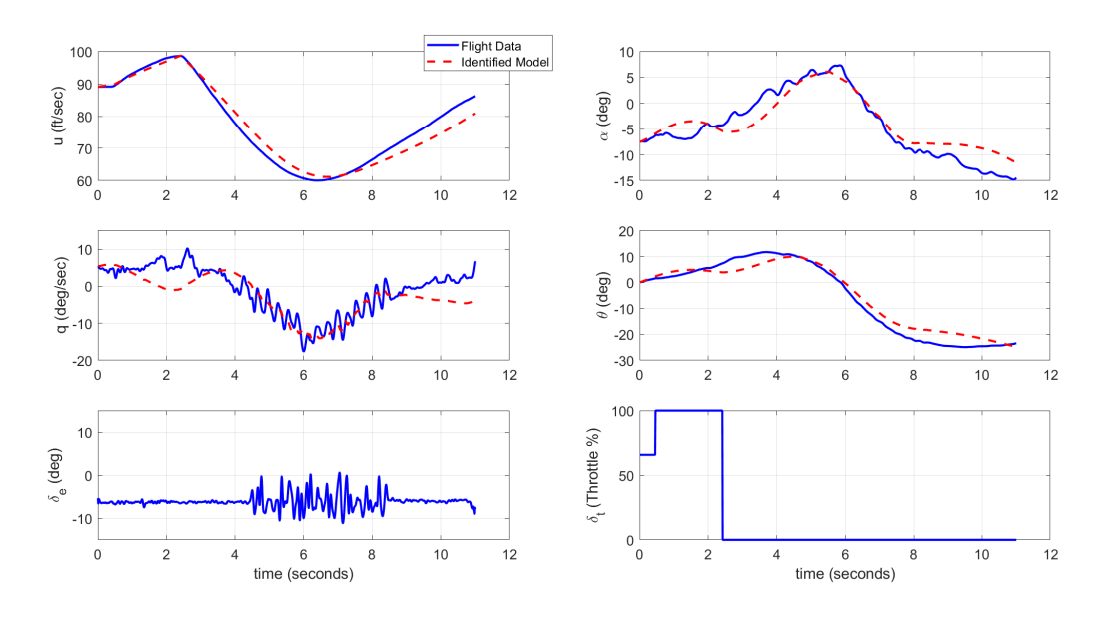


Fig. 5 State measurement and control input data used to identify model shown in Table 3

B. Lateral/Directional

Table 4 shows the identified lateral/directional model. Automated sine sweeps are injected to the aileron and rudder simultaneously. OKID identifies the standard lateral/directional dynamic modes. All of the identified modes are stable.

All of the MSV values are above 45% indicating that injected signals did a reasonable job of exciting the modes. Figure 4 shows the control inputs and state measurement data used to identify the model in Table 4. It is seen that the identify model matches the flight data well. The averaged TIC value is calculated to be 0.3080, which is slightly above the previously specified bound of 0.3 for an identified model to be considered a good quality model.

Table 4 Identified Lateral/Directional Anaconda Model

Mode	Eigenvalue	ω_n (rad/sec)	ζ	τ (sec)	MSV (%)	MCI (%)	MOI (%)
Roll	-2.6609	_	_	0.3758	45.3	100.0	58.5
Spiral	-0.2058	_	_	4.8591	100.0	22.3	100.0
Dutch Roll	$-1.1352 \pm j4.5260$	4.6662	0.2433	_	73.3	77.3	85.3

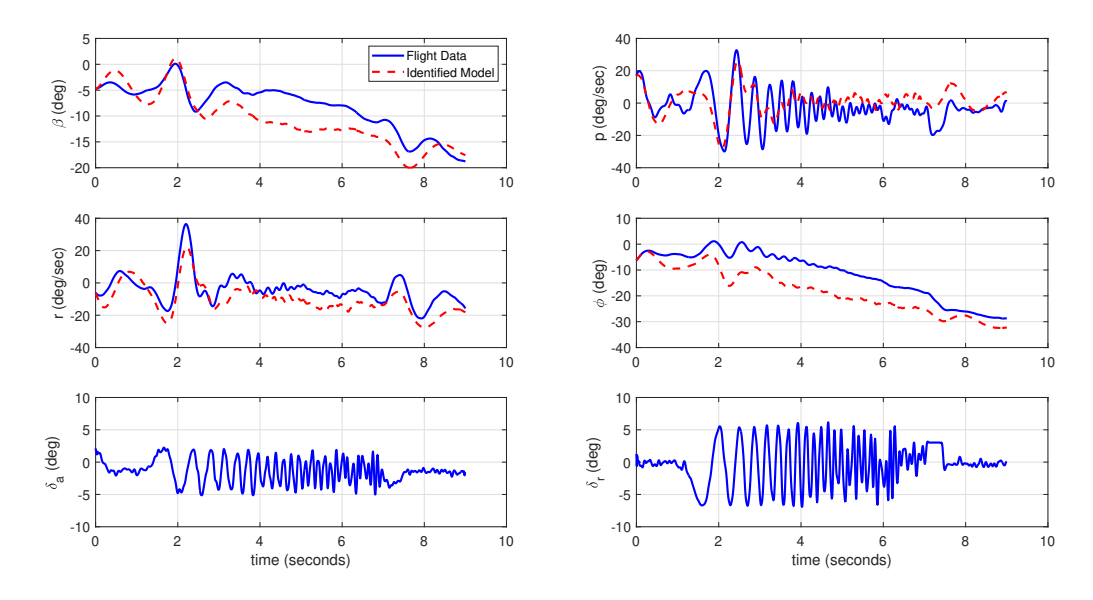


Fig. 6 State measurement and control input data used to identify model shown in Table 4

C. Combined Longitudinal Lateral/Directional

Table 5 shows the identified combined longitudinal lateral/directional model. A step input is first injected into the throttle. Theb automated sine sweeps with varying ranges are injected into the aileron, elevator and rudder. The aileron sweep lasts 6 seconds while the rudder and elevator sweeps last 3 seconds. OKID identifies all of the standard dynamic modes, corresponding to the results for the decouple models. The spiral and phugoid modes for the combine model match well with the spiral and phugoid modes identified in the decoupled models. Note that the identified spiral and phugoid modes in Table 5 have the highest MSV values. There are some similarities between the combined and decoupled for the other three modes, but these similarities are not as great as the spiral and phugoid modes. Note that MSV values for the short period, roll and dutch roll in Table 5 are below 30%. Figure 7 shows the control inputs and state measurements used to identify the model in Table 5. It is seen that there is reasonable matching between the flight data and the identified model. The averaged TIC value for identified combined model is calculated to be 0.3066, which is just above the specified bound of 0.3 in order for the identified to be considered a good quality model.

Table 5 Identified Combined Longitudinal Lateral/Directional Anaconda Model

Mode	Eigenvalue	ω_n (rad/sec)	ζ	τ (sec)	MSV (%)	MCI (%)	MOI (%)
Short Period	$-0.4595 \pm j2.6307$	2.6706	0.1721	_	14.2	55.2	69.3
Phugoid	$-0.0512 \pm j0.7385$	0.7403	0.0691	_	100.0	27.1	78.9
Roll	-1.0718	_	_	0.9330	29.3	55.2	69.3
Spiral	-0.2175	_	_	4.5977	84.2	100.0	64.3
Dutch Roll	$-1.3986 \pm j5.7871$	5.9537	0.2349	_	10.9	9.2	74.0

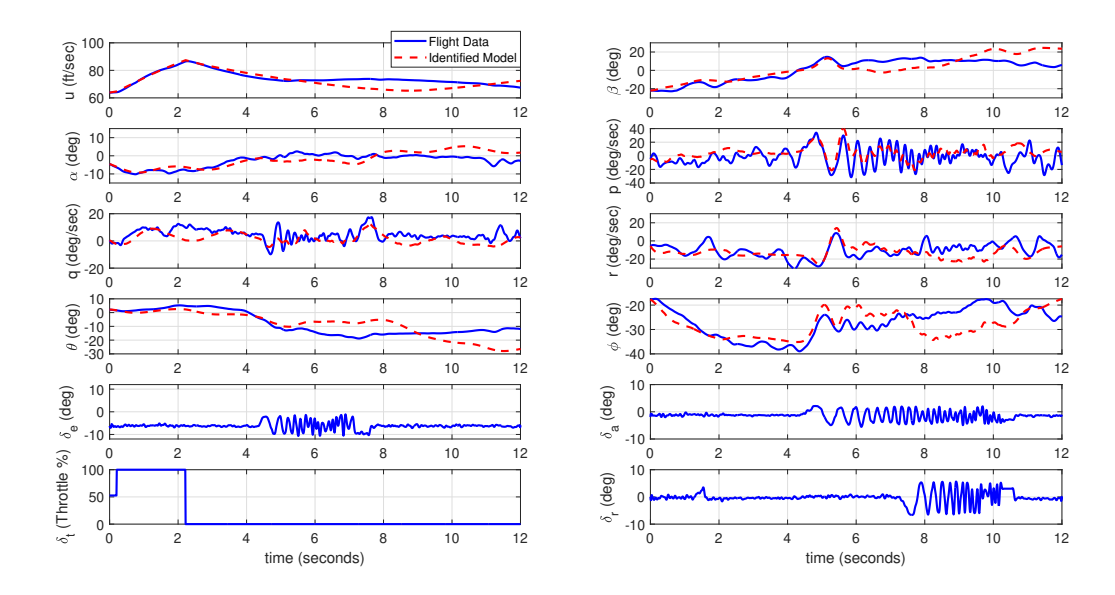


Fig. 7 State measurement and control input data used to identify model shown in Table 5

D. Comparison to UAS with Standard Empennage Configuration

The identified results for the RMRC Anaconda, which has an inverted V-Tail, are now compared to the identified results for Hangar-9 1/4-Scale PA-18 Super Cub, which has a standard empennage, presented in $\boxed{14}$. The short period damping for the Super Cub is 0.92 while for the Anaconda it is 0.183. The natural frequencies of the short periods are similar between the two vehicles however. The phugoid of the Anaconda has a natural frequency roughly four times larger that of the phugoid of the Super Cub. Additionally the damping for the phugoid of the Anaconda is approximately 3 times smaller than phugoid of the Super Cub. The lateral/directional modes of the Anaconda all have higher natural frequencies than the corresponding modes of the Super Cub. The damping on the dutch roll of the Anaconda is about three times smaller than the dutch roll damping for the Super Cub. In terms of the control influence matrices, the elevator control power on body-axis pitch rate q has a negative sign for both the Anaconda and Super Cub. The signs are opposite for the rudder power on body-axis yaw rate r however. This is likely due to how positive deflections are defined for the ruddervators.

IX. Conclusions

This paper presented an approach for generating linear time invariant state-space models using a flight test instrumentation system based on the robot operating system. Continuous-time linear state-space models were identified using the Observer/Kalman Identification algorithm with the flight data collected by the instrumentation system. Both manual and automated excitation maneuvers were used to generate models. Based upon the results in the paper the following conclusions can be drawn:

- 1) The excitation signal set used to identify the longitudinal model excite the longitudinal dynamics well generating a model with an averaged Theil Inequality Coefficient value of 0.153 and Mode Singular Values above 58%.
- 2) The excitation signal set used to identify the lateral/directional model excites the lateral/directional modes well with Mode Singular Values all above 45% but more accurate lateral/directional dynamics can be obtain as the averaged Theil Inequality Coefficient value was 0.308, which is slightly above the limit of 0.3 for a good model.
- 3) The excitation signal used to identify the fully combined model only sufficiently excited the short period and spiral modes of the vehicle with those modes having Mode Singular Values above 84% while the other modes while the other modes have Mode Singular Values below 30%. The Mode Singular Values along with a averaged Theil Inequality Coefficient value of 0.3066 means a more accurate fully combined model can be obtained.

Future work will include testing new excitation signal sets for the lateral/directional and combined longitudinal lateral/directional models and implementing an online identification node in the Developmental Flight Test Instrumentation Two system.

X. Acknowledgements

This work has been funded by the Center for Unmanned Aircraft Systems (C-UAS), a National Science Foundation Industry/University Cooperative Research Center (I/UCRC) under NSF award Numbers IIP-1161036 and CNS-1946890, along with significant contributions from C-UAS industry members.

Appendix

A. Identified Longitudinal Anaconda Model

The state vector is defined as $\mathbf{x} = [u, \alpha, q, \theta]^T$ with units of ft/sec, rad and rad/sec, respectively. The control vector is defined as $\mathbf{u} = [\delta_e, \delta_t]^T$, where δ_e is in rad and δ_t is the fraction of maximum throttle. The day of the flight the winds are calm. The trim values are as follows: $u_1 = 92.76$ ft/sec, $\alpha_1 = -6.33$ deg, $q_1 = -4.51$ deg/sec, $\theta_1 = 2.32$ deg, $\delta_{e_1} = -5.35$ deg, $\delta_{t_1} = 0.66$. The identified state and control influence matrices are

$$A = \begin{bmatrix} -0.0776 & 7.8530 & 1.5754 & -34.0312 \\ 0.00064253 & 1.0643 & 1.1486 & -0.3064 \\ -0.0090 & -3.8878 & -1.3847 & 1.4097 \\ -0.00033202 & -0.2522 & 0.8345 & 0.0769 \end{bmatrix}$$
$$B = \begin{bmatrix} 0.0998 & 14.9639 \\ -0.4515 & -0.0400 \\ -4.6956 & -0.0701 \\ -0.1946 & -0.0261 \end{bmatrix}$$
(15)

B. Identified Lateral/Directional Anaconda Model

The state vector is defined as $\mathbf{x} = [\beta, p, r, \phi]^T$ with units of rad and rad/sec, respectively. The control vector is defined as $\mathbf{u} = [\delta_a, \delta_r]^T$, where δ_a and δ_r are in rad. The winds are calm the day of the flight. The trim values are as follows: $\beta_1 = -5.79 \text{ deg}$, $p_1 = -1.1 \text{ deg/sec}$, $p_1 = -1.43 \text{ deg/sec}$ $\phi_1 = -3.86 \text{ deg}$, $\delta_{a_1} = -2.02 \text{ deg}$, $\delta_{r_1} = -0.62 \text{ deg}$. The identified state and control influence matrices are

$$A = \begin{bmatrix} -0.5376 & -0.0769 & -0.8559 & 0.7964 \\ -5.2769 & -2.7249 & 5.8739 & -2.9288 \\ 7.6818 & -2.0321 & -1.8385 & -2.4446 \\ -0.1237 & 0.9225 & 0.1135 & -0.0360 \end{bmatrix} B = \begin{bmatrix} 1.0966 & -0.2684 \\ 34.9671 & -1.9390 \\ -14.8447 & 3.7482 \\ 3.4265 & -0.2956 \end{bmatrix}$$
(16)

C. Identified Combined Longitudinal Lateral/Directional Anaconda Model

The state vector is defined as $\mathbf{x} = [u, \alpha, q, \theta, \beta, p, r, \phi]^T$ with units of ft/sec, rad and rad/sec, respectively. The control vector is defined as $\mathbf{u} = [\delta_e, \delta_t], \delta_a, \delta_r]^T$, where $\delta_e, \delta_a, \delta_r$ are in rad and δ_t is in fraction of maximum throttle. The day of the flight the winds 6.5 mpg with gusts of 7.7 mph. The trim values are as follows: $u_1 = 63.84$ ft/sec, $\alpha_1 = -4.54$ deg, $\theta_1 = 0.45$ deg, $q_1 = 2.17$ deg/sec, $\beta_1 = -21.2$ deg, $p_1 = -4.70$ deg/sec, $p_1 = -5.72$ deg/sec $p_1 = -17.67$ deg $p_1 = -6.23$ deg, $p_1 = -6.23$ deg, $p_1 = -1.91$ deg, $p_1 = -0.03$ deg. The identified state matrix and control influence matrix are

$$A = \begin{bmatrix} -0.1174 & 3.1684 & 4.2006 & -23.9637 & -5.7074 & -1.2649 & -0.1081 & -6.3103 \\ 0.0027 & -0.2125 & 0.8617 & 0.2263 & 0.3335 & -0.0324 & 0.0559 & -0.2735 \\ -0.0310 & -6.8413 & -0.5927 & -2.0019 & 0.2421 & 0.6814 & 0.5978 & -2.0724 \\ -0.00045898 & -0.2003 & 0.8178 & -0.1182 & 0.0100 & 0.0073 & 0.4806 & 0.1455 \\ 0.000087825 & -0.3246 & 0.1275 & -0.0875 & -0.0887 & -0.0047 & -1.5193 & 0.5430 \\ -0.0447 & -1.2918 & -2.2435 & -7.6262 & -3.5357 & -2.4595 & 7.4360 & -11.0421 \\ 0.0097 & -6.1893 & -2.5032 & 5.3016 & 6.1473 & -1.8948 & -1.3763 & 1.3214 \\ -0.0015 & -0.1031 & 0.0205 & -0.3871 & -0.0828 & 0.9250 & -0.0256 & -0.1427 \end{bmatrix}$$

$$B = \begin{bmatrix} 1.6577 & 16.3190 & -6.5871 & -0.7567 \\ -0.6530 & -0.00013824 & -0.0473 & 0.0987 \\ -7.7185 & -0.0633 & -2.2209 & -0.1899 \\ -0.4489 & 0.0249 & -0.0816 & 0.0504 \\ -0.0688 & -0.0217 & 1.2810 & 0.0351 \\ 0.103 & -0.1421 & 49.5231 & 6.3630 \\ 1.3289 & 0.3618 & -9.5430 & 2.2781 \\ -0.2895 & -0.0372 & 4.8701 & 0.8325 \end{bmatrix}$$

References

- [1] Finck, R. D., et al., "USAF Stability and Control DATCOM," Tech. Rep. AFWAL-TR-83-3048, Flight Dynamics Laboratory, Wright Aeronautical Laboratories, Wright-Patterson AFB, OH, Apr. 1978. URL http://www.dtic.mil/docs/citations/ADB072483
- [2] Roskam, J., Airplane Flight Dynamics & Automatic Flight Controls: Part I, DARCorporation, 2001.
- [3] Albright, A. E., Dixon, C. J., and Hegedus, M. C., "Modification and Validation of Conceptual Design Aerodynamic Prediction Method HASC95 With VTXCHN," Tech. Rep. NASA Contractor Report 4712, NASA Langley Research Center, Mar. 1996. URL https://ntrs.nasa.gov/search.jsp?R=19960022946
- [4] Player, J., and Gingras, D. R., "Rapid Simulation Development for Evaluation of Conceptual Unmanned Aerial Vehicles," *AIAA Modeling and Simulation Technologies Conference and Exhibit*, AIAA, Providence, RI, 2004. doi:10.2514/6.2004-5042.
- [5] Juang, J.-N., and Pappa, R. S., "An eigensystem realization algorithm for modal parameter identification and modal reduction," *Journal of Guidance, Control, and Dynamics*, Vol. 8, No. 5, 1985, pp. 620–627. doi:10.2514/3.20031, URL http://dx.doi.org/10.2514/3.20031
- [6] Juang, J.-N., Phan, M., Horta, L. G., and Longman, R. W., "Identification of observer/Kalman filter Markov parameters," *Journal of Guidance, Control, and Dynamics*, Vol. 16, No. 2, 1993, pp. 320–329. doi:10.2514/3.21006, URL http: //dx.doi.org/10.2514/3.21006
- [7] Tischler, M. B., and Cauffman, M. G., "Frequency-Response Method for Rotorcraft System Identification: Flight Applications to BO-105 Coupled Rotor/Fuselage Dynamics," *Journal of the American Helicopter Society*, Vol. 37, No. 3, 1992, pp. 3–17.
- [8] Juang, J.-N., Applied System Identification, Prentice Hall, Upper Saddle River, NJ, 1994.
- [9] Juang, J.-N., and Phan, M., "Identification of System, Observer, and Controller from Closed-loop Experimental Data," *Journal of Guidance, Control, and Dynamics*, Vol. 17, No. 1, 1994, pp. 91–96. doi:10.2514/3.21163, URL http://dx.doi.org/10 2514/3.21163
- [10] Hamel, P. G., and Jategaonkar, R. V., "Evolution of Flight Vehicle System Identification," *Journal of Aircraft*, Vol. 33, No. 1, 1996, pp. 9–28. doi:10.2514/3.46898, URL http://dx.doi.org/10.2514/3.46898
- [11] Woodbury, T., Valasek, J., and Arthurs, F., "Flight test results of Observer/Kalman Filter Identification of the Pegasus unmanned vehicle," AIAA Atmospheric Flight Mechanics Conference, Kissimmee, FL, 2015.

- [12] Arthurs, F., Valasek, J., and Zeigler, M. D., "Precision Onboard Small Sensor System for Unmanned Air Vehicle Testing and Control," AIAA Guidance, Navigation, and Control Conference, San Diego, CA, 2016. doi:10.2514/6.2016-1138, URL http://dx.doi.org/10.2514/6.2016-1138
- [13] Harris, J., Henrickson, J., Arthurs, F., and Valasek, J., "Aircraft System Identification using Artificial Neural Networks with Flight Test Data," 2016 International Conference on Unmanned Aircraft Systems (ICUAS'16), IEEE, Arlington, VA, 2016. doi:10.1109/ICUAS.2016.7502624.
- [14] Lu, H., Rogers, C., Goecks, V., and Valasek, J., "Online Near Real Time System Identification on a Fixed-Wing Small Unmanned Air Vehicle," 2018 AIAA Atmospheric Flight Mechanics Conference, 2018. doi:10.2514/6.2018-0295, URL https://arc.aiaa.org/doi/abs/10.2514/6.2018-0295
- [15] Leshikar, C., Eves, K., Ninan, N., and Valasek, J., "Asymmetric Quadrotor Modeling and State-Space System Identification," 2021 International Conference on Unmanned Aircraft Systems (ICUAS), IEEE, 2021, pp. 1422–1431.
- [16] Lu, H., Harris, J., Goecks, V. G., Bowden, E., and Valasek, J., "Flight test instrumentation system for small UAS system identification," 2017 International Conference on Unmanned Aircraft Systems (ICUAS), 2017, pp. 1696–1705. doi:10.1109/ ICUAS.2017.7991399.
- [17] Agha, M., Kanistras, K., Saka, P., Rutherford, M., and Valavanis, K., "System Identification of a Circulation Control UAV Using X-Plane Flight Simulation Software and Flight Data," 2017 AIAA Modeling and Simulation Technologies Conference, 2017. doi:10.2514/6.2017-3154, URL https://arc.aiaa.org/doi/abs/10.2514/6.2017-3154
- [18] Valasek, J., and Chen, W., "Observer/Kalman Filter Identification for Online System Identification of Aircraft," *Journal of Guidance, Control, and Dynamics*, Vol. 26, No. 2, 2003, pp. 347–353. doi:10.2514/2.5052, URL http://dx.doi.org/10/2514/2.5052.
- [19] Schroeder, M., "Synthesis of low-peak-factor signals and binary sequences with low autocorrelation (Corresp.)," *IEEE Transactions on Information Theory*, Vol. 16, No. 1, 1970, pp. 85–89.
- [20] Morelli, E. A., "Multiple input design for real-time parameter estimation in the frequency domain," *IFAC Proceedings Volumes*, Vol. 36, No. 16, 2003, pp. 639–644.
- [21] Jategaonkar, R. V., Flight vehicle system identification: a time domain methodology, American Institute of Aeronautics and Astronautics, 2006.
- [22] Longman, R., Bergmann, M., and Juang, J.-N., "Variance and bias confidence criteria for ERA modal parameter identification," Astrodynamics Conference, 1988, p. 4312.